Journal of Polymers and the Environment
https://doi.org/10.1007/s10924-018-1197-4

ORIGINAL PAPER

Water Remediation: PVA-Based Magnetic Gels as Efficient Devices to Heavy Metal Removal

María Pía Areal[1] · M. Lorena Arciniegas[1] · Fernanda Horst[2] · Verónica Lassalle[2] · Francisco H. Sánchez[3] · Vera A. Alvarez[1] · Jimena S. Gonzalez[1]

Abstract

Scientific and technological researches are devoted to obtain materials capable of retaining different kinds of pollutants, contributing to contamination solutions. In this context, hydrogels have emerged as great candidates because of their excellent absorption properties as well as good mechanical, thermal and chemical properties. More specifically, ferrogels (magnetic gels) present the extra advantage of being easily manipulated by a permanent magnet. Here, we present the results derived from the application of ferrogels as efficient tools to extract heavy metal pollutants from wastewater samples. The gels were prepared following the method of freezing and thawing of a polyvinyl alcohol aqueous solution with magnetic nanoparticles coated with polyacrylic acid. Ferrogels were fully characterized and their ability to retain Cu^{2+} and Cd^{2+}, as model heavy metals, was studied. Thus kinetics and mechanisms of adsorption were evaluated and modeled. The concentration of MNPs on the PVA matrix was key to improve the adsorption capability (approximately the double of retention is improved by the MNPs addition). The adsorption kinetics was determined as pseudo-second order model, whereas the Langmuir model was the most appropriate to explain the behavior of the gels. Finally reuse ability was evaluated to determine the real potential of these materials, the ferrogels demonstrated high efficiency up to about five cycles, retaining about 80–90% of their initial adsorption capability. All the results indicated that the materials are promising candidates able to compete with the commercial technology regarding to water remediation.

Keywords Ferrogel · Heavy metal removal · Freeze–thaw · Magnetic gel · PVA

Introduction

During the last decades, natural resources have been greatly deteriorated. Water resources are ones of the most affected, since high polluted areas have greatly advanced [1]. Among common contaminants, heavy metals cause severe damage to the health of living beings. Different recovery techniques have been developed to clean contaminated waters. The most common works are through physical, chemical, biological principles or a combination of them [2]. Technological development currently aims to obtain materials able to retain contaminants with high efficiency in short times and also in economical way [3, 4]. In this context, hydrogels have emerged as great candidates for these issues because of their excellent absorption properties as well as good mechanical, thermal and chemical properties [5]. Hydrogels are soft networks with interstitial fluid, able to absorb huge amounts of water or biological fluids [6–8]. Composite polyvinyl alcohol (PVA) hydrogels, obtained by the freezing and thawing

Electronic supplementary material The online version of this article (https://doi.org/10.1007/s10924-018-1197-4) contains supplementary material, which is available to authorized users.

✉ Jimena S. Gonzalez
jimena.gonzalez@fi.mdp.edu.ar

[1] Institute of Materials Science and Technology (INTEMA), University of Mar del Plata and National Research Council (CONICET), Colón 10890, 7600 Mar del Plata, Argentina

[2] Institute of Chemistry of South (INQUISUR), South National University, National Research Council CONICET, CC 717, 8000 Bahía Blanca, Argentina

[3] Physics Department – Physics Institute of La Plata (IFLP – FCE), University of La Plata, National Research Council CONICET, CC 67, 1900 La Plata, Argentina

Published online: 08 February 2018

(F/T) method, have proved to be very efficient as adsorbents of Hg, phosphates, Cu, and Cd, among other contaminants [9].

Magnetic composites have also been widely used in wastewater treatment and biomedical drug delivery [10–14] or protein adsorption [15], due to their low toxicity, good biocompatibility, easy separation, and ability to be controlled by a magnetic field (remote control) [16]. Magnetic gels, also called ferrogels (FGs), are magnetic-field-sensitive gels, which are obtained by dispersing magnetic particles of colloidal size into a crosslinked polymer [17]. Major advances have been reached through surface modification of these nanoparticles. This is achieved by the attachment of organic or inorganic molecules, which not only stabilizes the nanoparticles, eventually preventing their oxidation, but also provides specific functionalities that can be selective for ion uptake [18].

In the last years, many hydrogels and composite hydrogels have been examined for potential applications as heavy metal adsorbents. The poly(sodium acrylate)–graphene oxide double network hydrogel, for example, has been found to have maximum sorption capacities of up to 238.3 and 165.5 mg/g at pH 6 and T = 303 K, for Cd(II) and Mn(II), respectively, estimated from the Langmuir model [19]. Moreover, two types of degradable poly(propylene glycol) hydrogels have been found to be suitable for the adsorption of heavy metals. These authors reported that the amounts of adsorbed metal ions increase with the initial metal ion concentration and hydrogel dosage; but decrease with temperature [20]. Also, renewable poly(amidoamine)/hemicellulose hydrogels have been prepared and shown high adsorption capacity for Cu^{2+}, Cd^{2+}, Pb^{2+}, Zn^{2+}, Ni^{2+}, and Co^{v} [21]. Moreover, hydrogel based on agricultural waste was developed for removal of Congo red and methyl orange dyes from wastewater, and the adsorption of dyes increased with increasing temperature [22].

The aim of this work is to explore the use of PVA ferrogel, as efficient tools for the remediation of wastewater. In particular, the work has focused in heavy metals as pollutants, using Cu and Cd ions as models. To this purpose polyacrylic acid (PAA) coated magnetite nanoparticles (MNPs) were added in a PVA solution and then crosslinked using the freezing and thawing technique. Then the ability to these materials to eliminate heavy metals from aqueous solution of both heavy metals was studied in batch. The kinetics and the mechanisms of adsorption were evaluated. The influence of the concentration of MNPs into the FGs, on the adsorption capability was also explored. Finally, reuses assays were implemented to determine the real potential of these materials. Currently, there are not reported articles working with the system PVA/PAA-MNPs/heavy metal ions including in the present contribution.

Materials and Methods

Preparation of Hydrogel and Ferrogel Samples (Fig. 1)

PVA hydrogels were obtained by four cycles of freezing–thawing (F/T) applied on 10 wt% PVA aqueous solutions (89,000–98,000 g/mol, Sigma-Aldrich). PVA ferrogels (FGs) were obtained using the F/T technique; MNPs coated with PAA (provided by NANOGAP, particle size approximately 10 nm) were incorporated to the 10 wt% PVA aqueous solution, in order to obtain 1, 3, 6, and 9% of MNPs by weight of polymer content. Then, four cycles of F/T were performed.

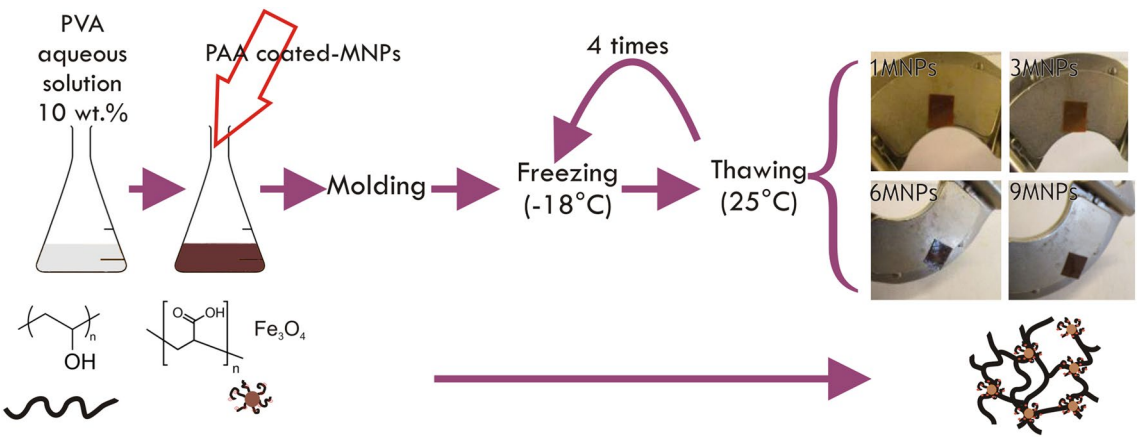

Fig. 1 Scheme of samples preparation

Morphological, Physical, Chemical and Thermal Characterization of the Samples

Field emission scanning electron microscopy (FESEM) was employed to characterize morphologies. FESEM images were obtained using a JEOL JSM-6460 LV instrument. Samples were cryo-fractured by a previous immersion in liquid N_2 and coated with gold before testing.

For their physical–chemical characterization, the hydrogel and ferrogel samples were dried for 48 h at room temperature and differential scanning calorimetric measurements were carried out in a TA Q 2000 instrument. The samples were heated from room temperature to 260 °C at 10 °C/min, under a N_2 atmosphere. The melting temperature (T_m) and crystallinity degree were determined from the resulting thermograms. The crystallinity degree was calculated from Eq. 1,

$$X_{cr}\% = \frac{\Delta H}{\Delta H^0 \times W_{PVA}} \times 100 \quad (1)$$

where ΔH was determined by integrating the area under the melting peak over the 190–240 °C range, ΔH^0 is the theoretical heat required for melting a 100% crystalline PVA sample (138.6 J/g) [23] and W_{PVA} is the weight fraction of PVA in the ferrogel.

Thermogravimetric (TGA) studies were performed in a TA Q500 instrument from room temperature to 900 °C at 10 °C/min under air atmosphere. The degradation temperature (T_p) and iron oxide content, reported as the fully oxidized crystalline phase, Fe_2O_3, (Fe_2O_3 wt%) were obtained from these measurements.

The gel fraction (GF%) was measured as follows: the initial weight of the gels was recorded, and then the gels were submerged in distilled water for 4 days to reach equilibrium swelling. Finally, the samples were dried at 30 °C to reach constant weight. GF% was determined using Eq. 2:

$$GF\% = \frac{W_f - W_{Fe}}{W_i - W_{Fe}} \quad (2)$$

where W_i is the initial weight of the gel and W_f is the weight after the gels were dried. With ferrogel samples, the weight content of iron, W_{Fe}, must be considered and was determined by TGA measurements.

Swelling determinations were carried out in phosphate buffers at pH 4 and 7, in the presence and in the absence of a magnetic field. The equilibrium swelling degree (W_∞ %) was determined by Eq. 3:

$$W_\infty\% = \frac{W_f - W_i}{W_i} \times 100 \quad (3)$$

where W_i is the weight of the samples before immersion and W_f is the weight of the sample at equilibrium.

X-Ray diffraction (XRD) tests were carried out to identify the magnetic phase inside the polymer matrix. XRD were performed using an X-Pert Pro diffractometer, operating at 40 kV and 40 mA, with CuKα radiation (λ = 0.154 nm). All samples were scanned in 2θ = 2°–50° at 2°/min.

Magnetic Characterization of the Ferrogel

The magnetic properties (measurements of mass magnetization (M) vs. magnetic field (MF) and measurements of M vs. temperature after zero field cooling (ZFC) and field cooling (FC) from room temperature) were determined with a VSM LakeShore 7404 magnetometer and with a MPMS-XL superconducting quantum interference device (SQUID) from Quantum Design, Inc.

ZFC and FC measurements were performed under a field of 0 or 100 Oe as a function of temperature in the range between 10 and 300 K. The ferrogel was first measured in its dry state and then in a completely hydrated state. In the second case, during the final part of the ZFC measurement and the initial part of the FC protocol, temperatures were kept below water liquefaction point in order to avoid potential out of equilibrium melting/freezing phenomena. The experimental time window for M measurements in the SQUID was estimated to be about 100 s.

Heavy Metal Adsorption Assays

Cu(II) and Cd(II) kinetics absorption studies were carried out in batch using aqueous solutions of each metal in a concentration of 100 mg/L. The quantification of the adsorbed metals was carried out indirectly by measuring the ion concentration in the solution by atomic absorption using a GBC Scientific Equipment. Equilibrium isotherm studies were performed at 20 °C, varying the initial concentration of metal in the solution from 5 to 100 mg/L at pH 5. The amount of adsorbed ions, expressed as mg per gram of gel, q_e, was obtained by using Eq. 4:

$$q_e = (C_i - C_e) \times \frac{V}{W} \quad (4)$$

where C_i and C_e are initial and equilibrium concentrations, respectively, in mg/L. W is the dry mass of adsorbent (mg) and V is volume of solution in L. The adsorption data was fitted using Langmuir and Freundlich models.

Reusability Studies

The ability of the ferrogels to be regenerated and reused was investigated by performing five successive adsorption–desorption cycles in distilled water. Samples were loaded in the heavy metal solutions (100 mg/L) during 1 h, then washed

superficially with distilled water and placed in distilled water for 1 h.

Recovery% was calculated as: (q_e firth cycle/q_e first adsorption assay) × 100.

Results and Discussion

Characterization of the Ferrogels

Thermal, chemical and physical properties of the ferrogeles are summarized in Table 1.

The TGA measurements, which allowed corroborating the iron content, showed that the desired amount of iron oxides was incorporated to the ferrogels. Also, an increase in the degradation temperature was evidenced, demonstrating the suitable interaction between the –OH groups from PVA and the –COOH present in the MNPs-PAA coating [24]. This behaviour may be ascribed to restrictions in the mobility of polymeric chains and a good interaction between the MNPs and the hydrogel.

GF % is a relative determination of the crosslinking degree. The good interaction between the PVA and PAA chains may imply a lower crosslinking degree, justifying the decrease in GF % with the increase in MNP content [25].

From the XRD spectra (Fig. 2) it can be observed the 19.8° and 22.9° (2θ) peaks corresponding to the semicrystalline polymer (PVA) [26]. Moreover, the MNPs and ferrogels present a characteristic peak in 35.5° (2θ) for the maghemite or magnetite (*9-0629 JCPDS-standard card for magnetite*).

The results on swelling degree are presented in Table 2.

The analysis in various media allowed determining different behaviors. At a same pH, the increase in W_∞ with the MNPs content could be attributed to a more porous microstructure, derived from the decrease in GF [27]. From pH 4 to 7, W_∞ increased considerably, which could be attributed to the complete ionization of the –COOH groups present in the PAA coating (PAA pka = 4.5) [28].

Finally, a decrease in W_∞ was evidenced when a MF was applied, determining that a MF could increase the stiffness of the ferrogels and tended to close the pores. Other authors have attributed this decrease to the alignment of MNPs in the material, which forms a barrier that prevents molecules to diffuse [29].

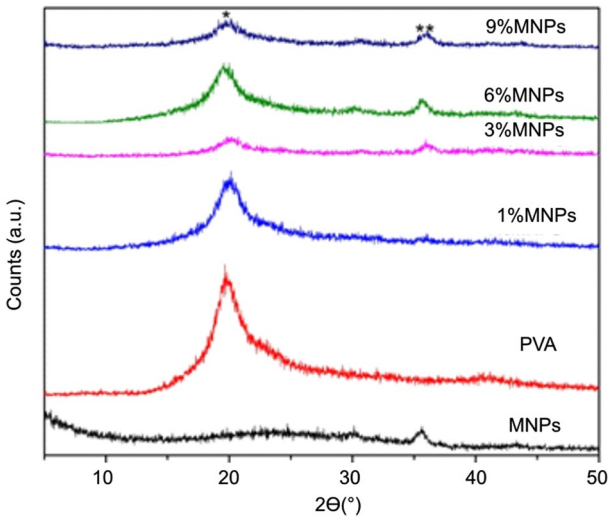

Fig. 2 XRD spectra of MNPs, PVA hydrogel and PVA ferrogels with different MNPs contents

Magnetic Characterization of the Samples

The potential of a magnetic material in certain applications may be evaluated by analyzing the magnetization curve (M vs. H). The curves obtained for 1, 6, and 9% MNPs ferrogels are shown in Fig. 3.

The Ms appears to be independent on the amount of magnetic particles incorporated in the PVA matrix since the values of Ms were almost similar between 65.9 and 67.3 emu/g. Similar values have been reported for magnetite-coated particles [16]. The value reported for magnetite (Fe_3O_4) nanoparticles with similar size distribution is of 92 emu/g [30]. The lower M_s values of the MNPs could be attributed to the superficial disorder caused by the presence of the PAA coating and defects and impurities of the crystal structure [18, 25].

Table 1 Melting temperature (T_p), iron content (Fe_2O_3 wt%), gel fraction (GF%) and crystallinity degree (Xcr%) of hydrogel and ferrogels with different content of MNPs

Sample	Fe_2O_3 (wt%)	T_p (°C)	GF (%)	X_{cr} (%)
PVA	–	295.8	99.5 ± 0.5	54.6 ± 0.8
1% MNPs	1.39	319.2	95.8 ± 3.5	45.8 ± 3.5
3% MNPs	4.19	320.3	91.5 ± 2.8	42.6 ± 0.7
6% MNPs	7.01	318.6	89.7 ± 6.5	41.5 ± 1.4
9% MNPs	9.34	322.6	80.1 ± 11.4	39.0 ± 0.9

Table 2 Swelling equilibrium capacity of PVA hydro and ferrogels with different contents of MNPs, as a function of the pH and in the presence of a permanent magnetic field (MF)

M_∞ %			
Sample	pH 4	pH 7	pH 7 MF
PVA	262.6 ± 33.8	259.3 ± 12.3	–
1% MNPs	276.2 ± 23.6	305.6 ± 50.6	219.6 ± 9.5
3% MNPs	294.1 ± 13.8	383.6 ± 5.2	230.4 ± 26.5
6% MNPs	346.6 ± 9.5	402.2 ± 14.3	356.8 ± 16.7
9% MNPs	359.9 ± 4.9	404.6 ± 15.6	320.5 ± 21.2

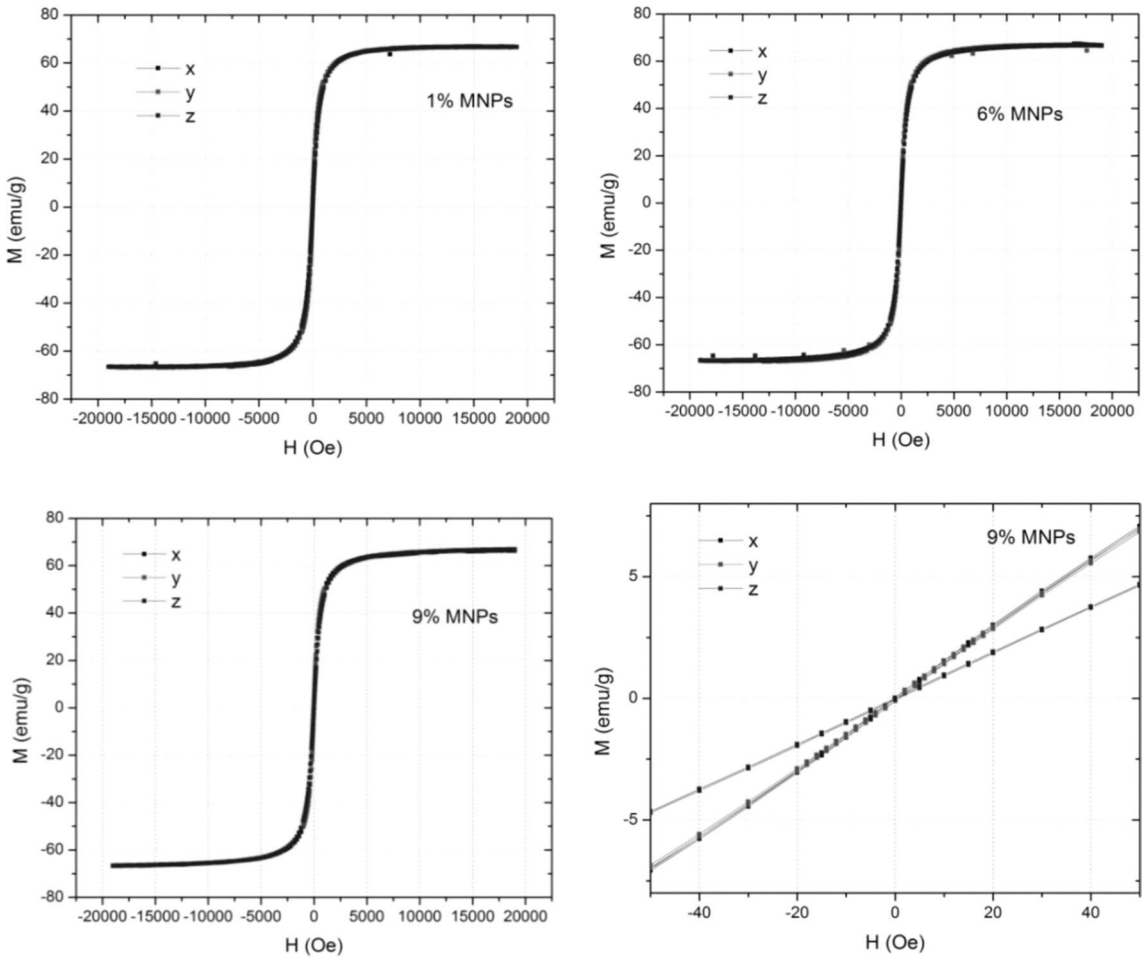

Fig. 3 Magnetization curve obtained for ferrogels of 1% MNPs, 6% MNPs, 9% MNPs; and magnetic susceptibility of 9% MNPs ferrogel

The samples presented low coercivity (H_c): 4.95; 1.38 and 2.98 Oe for 1, 6 and 9% MNPs ferrogels respectively at room temperature (300 K). This means that the MNPs had a superparamagnetic behavior at 300 K [31]. In fact, coercivity was significant only for the 1% sample since the typical error of VSM field recorded was of about 1–2 Oe.

A deeply discussion regarding to the magnetic properties of the prepared materials may be found in Supplementary Material.

The morphological study by FESEM firstly revealed a highly porous structure (Fig. 4a, b) with particles into the pore. It also showed the presence of nanoparticle clustering. These structures appear to be independent on the MNPs concentration in the polymeric matrix (see Fig. 4c, d). This morphology may partially justify some data associated to the magnetic behavior (see Supplementary Fig. S1).

Determination of Adsorption Capability

The results obtained from the adsorption of Cu^{2+} and Cd^{2+} are presented in Fig. 5, in terms of the amount of metal ion adsorbed (mg) per g of adsorbent as a function of the contact time. The trend observed by varying the MNPs concentration in the ferrogel matrix was analyzed and included in Fig. 5. The adsorptions proceed quickly, reaching the adsorption equilibrium after 20 min of being in contact with the ion solution. The data from the adsorption equilibrium capacity (q_e) are displayed in Table 3, similar q_e values were obtained in guar gum-g-(acrylic acid-coacrylamide-co-3-acrylamido propanoic acid) hydrogel [32] however, others hydrogels based on sodium alginate-g-poly(AMPS-co-AA-co-AM) showed maximun adsorption capacities of cadmium ions higher than our ferrogels (456.62 mg/g) [33].

These curves and their trend reveal that the higher adsorption capacity may be reached by increasing the initial

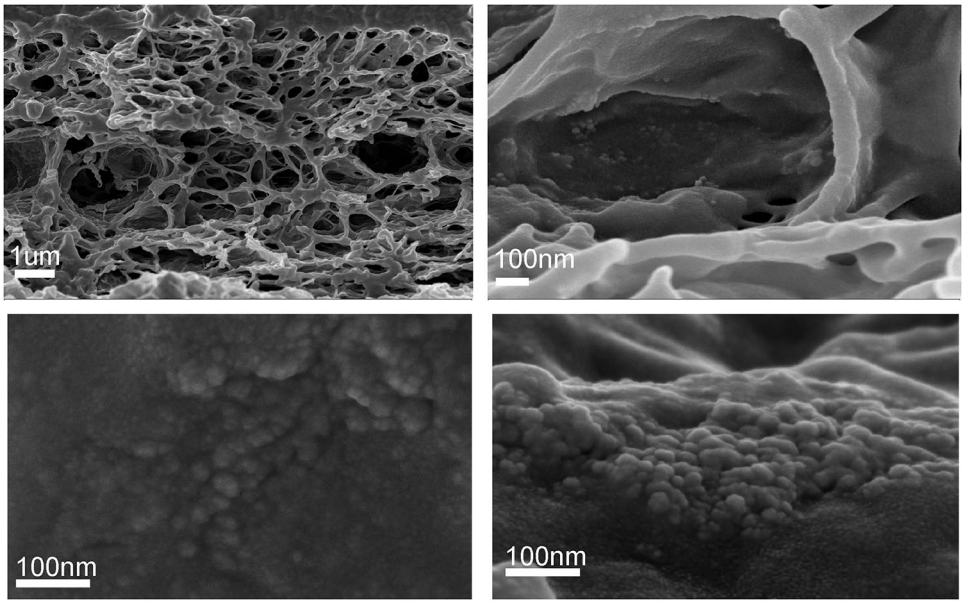

Fig. 4 FESEM image of ferrogels: **a** sample of 6% MNPs, **b** magnification of a pore of 6% MNPs, **c** magnification of 6% MNPs, **d** sample of 9% MNPS

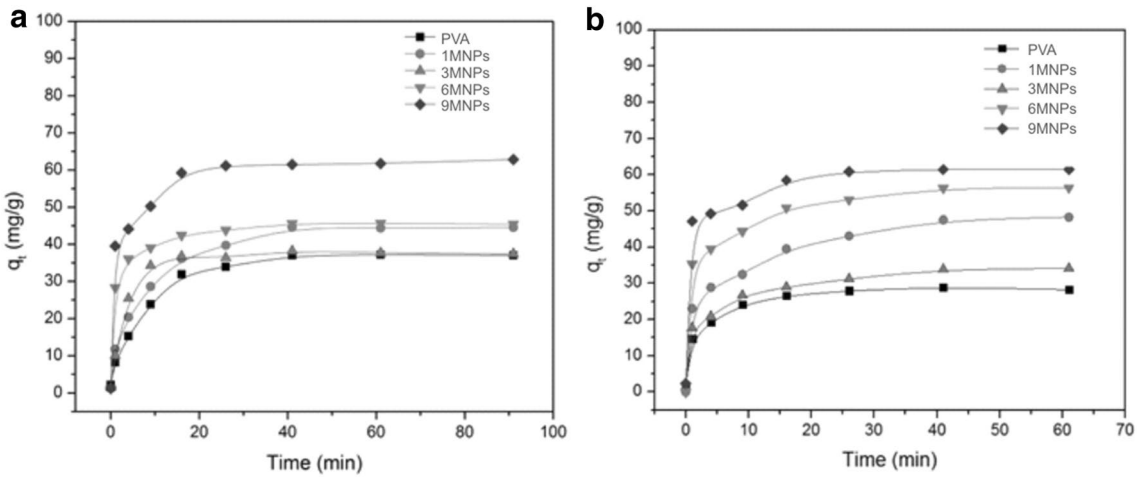

Fig. 5 Retention of ions in PVA hydrogel and ferrogels with different concentration of MNPs at pH 7 in a 100 mg/L of **a** Cu^{2+}, **b** Cd^{2+}

Table 3 Equilibrium absorption capacity of hydrogels and ferrogels of different MNP concentrations in solutions of Cu^{2+} and Cd^{2+}

Sample	q_e Cu^{2+} (mg/g)	q_e Cd^{2+} (mg/g)
PVA	28.6	36.4
1% MNPs	47.9	44.6
3% MNPs	33.7	37.4
6% MNPs	56.5	45.6
9% MNPs	61.5	62.4

concentration of MNPs in the FGs formulation. This phenomenon may be justified by the presence of PAA in the FGs moieties. Since at the pH fixed for the test, PAA was fully ionized, leaving available anionic sites (i.e. COO–) that may establish electrostatic interactions with the metallic cations. Similar behaviors have been previously evidenced using PAA/PVA membranes [34]. The selectiveness of magnetite against Cd and Cu ions was determined by the formation of coordinated bonds between Fe and the metal [35]. Hence, the adsorption might be attributed to a synergic effect of both phenomena.

The efficiency of adsorption achieved within this work is comparable to the data reported by other authors using PVA based gels [36] or chitosan/cellulose based gels [12].

Adsorption Kinetics

The study of the adsorption kinetics gives useful information about the adsorption efficiency and the adsorption

mechanisms. Lagergreen or pseudo-first order and pseudo-second order models were used to study the adsorption kinetics. The pseudo-first order model is defined as:

$$\ln(q_e - q_t) = ln\, q_e - \frac{k_1}{2.303}t \tag{5}$$

where q_e and q_t are the absorption capacities at the equilibrium and at time t, expressed as mg of adsorbed ions per g of gel (mg/g), and k_1 is the adsorption rate constant (min^{-1}). The value of this last quantity can be obtained from the curve.

The pseudo-second order model is presented by Eq. 6:

$$\frac{t}{q_t} = \left(\frac{1}{k_2 q_e^2}\right) + \left(\frac{1}{q_e}\right)t \tag{6}$$

where k_2 is the adsorption rate constant (min^{-1}), which can be obtained from the intercept of the graphic t/q_t versus t. These assays were performed with 9% MNPs because it demonstrated to be the most efficient ferrogel against metal adsorption, and also using the PVA hidrogel as reference.

According to the values of R^2 (R-Squared, the proportion of variability in a data set that is accounted for by a statistical model) displayed in Table 4, the pseudo second order was the model that better fits the achieved data. This determines that the rate-limiting may be due to chemical adsorption or to the formation of chemical bonds between adsorbent and adsorbate [37] in a monolayer on the surface, which could involve MNPs and the coating of PAA. Similar results were reported by other authors, where the first order model do not fit the adsorption process of hydrogels [36, 38].

Adsorption Isotherms

To understand the distribution of the heavy metal ions on the adsorbent surface and the adsorption process, it is necessary to study the adsorption isotherms. Empirical adsorption includes the Langmuir (Eq. 7) and the Freundlich (Eq. 8) models.

$$\frac{C_e}{q_e} = \frac{\left(C_e + \frac{1}{K_L}\right)}{q_m} \tag{7}$$

$$\log q_e = \log K_F + \frac{1}{n}\log C_e \tag{8}$$

where q_m is the maximum capability of the gel, K_L is the Langmuir constant (related to the adsorption rate), K_F is the Freundlich constant, which is related to the adsorption capability of the gel, and (1/n) represents the heterogeneity of the surface.

The Langmuir and Freundlich parameters are displayed in Table 5.

The adsorption process fitted well with the Langmuir model. Values of K_L similar to those displayed in Table 5 have been found by other authors [35, 39]. It is interesting to note that these hydrogels have higher retention capacity than chemically crosslinked hydrogel [38]. Similar parameter values have also been reported for Cu retention in chitosan magnetic hydrogels [35]. The adsorption mechanism could be mainly attributed to the formation of a single layer of ions on the hydrogel surface and on the active sites of the material [39]. As the concentration of MNPs increases, more functional groups (–COOH, exposed Fe) are available to interact with the ions of the solution, and thus more active sites, which could be occupied by metal ions, are present in the material.

Adsorption Mechanism

The adsorption process depends on the structural properties of the adsorbent (porosity, specific area, etc.), the properties of the metals in the solution, the concentration of the metal, and the interaction between the metal and the active sites of the adsorbent [36, 39]. The intraparticle diffusion is a progressive transport mechanism that implies the movement

Table 4 Pseudo first order and pseudo second order kinetic model parameters for adsorption of Cu^{2+} and Cd^{2+} of PVA hydrogel and 9% MNPs ferrogel

Pseudo first order model	Cu^{2+}			Cd^{2+}		
	q_e (mg/g)	k_1	R^2	q_e (mg/g)	k_1	R^2
PVA	18.66	0.15	0.977	54.22	0.31	0.882
9% MNPs	23.19	0.17	0.958	21.70	0.24	0.920
Pseudo second order model	q_e (mg/g)	k_2	R^2	q_e (mg/g)	k_2	R^2
PVA	29.96	0.0079	0.996	44.17	0.0042	0.996
9% MNPs	63.33	0.0134	0.999	54.76	0.0136	0.999

Table 5 Results obtained from Langmuir and Freundlich isotherm models for the retention of Cu^{2+} and Cd^{2+} in hydrogels and 9% MNPs ferrogel

Langmuir	Cu^{2+}			Cd^{2+}		
	q_m (mg/g)	K_L	R^2	q_m (mg/g)	K_L	R^2
PVA	66.36	1.30	0.997	90.50	0.17	0.995
9% MNPs	72.99	2.75	0.990	71.28	1.08	0.992
Freundlich	1/n	K_F (L/g)	R^2	1/n	K_F (L/mg)	R^2
PVA	0.89	1.41	0.982	0.95	1.42	0.968
9% MNPs	0.75	3.56	0.977	0.94	1.43	0.983

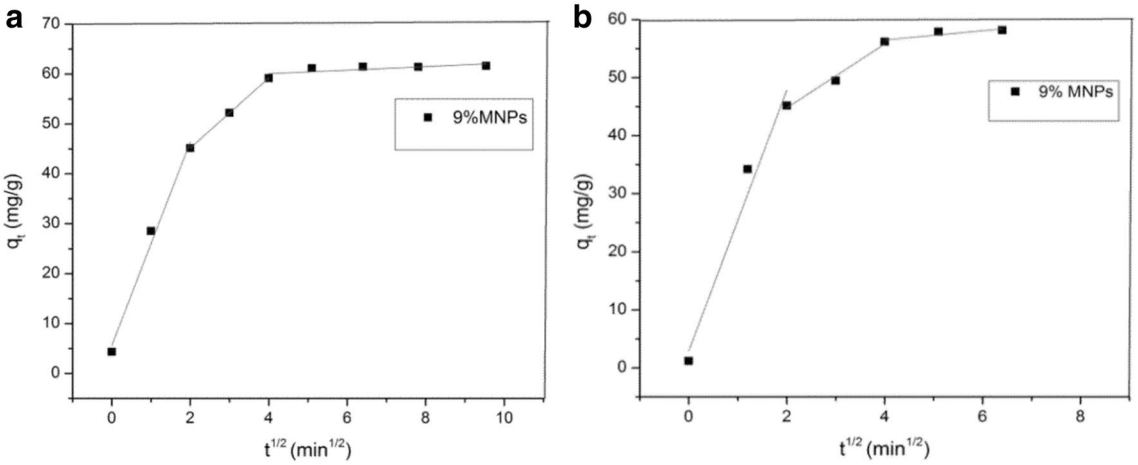

Fig. 6 Curve of q_t versus $t^{1/2}$, obtained througt the model of intraparticle diffusion: three steps of absorption for samples of 9% MNPs **a** in Cu^{2+} and **b** in Cd^{2+}

of ions from the bulk of the solution to the solid [36]. This model has been extensively used to simulate the behavior of porous materials.

The intraparticle difussion model (Eq. 9) gives information about the predominant mechanism during the initial phases of the process. If the plot obtained (q_t vs. $t^{1/2}$) is linear and intercepts the origin, then intraparticle diffusion is the controlling mechanism.

$$q_t = k_i\, t^{\frac{1}{2}} + C \tag{9}$$

The result of the fitting was a point distribution; three different linear zones could be determined (Fig. 6), meaning that intraparticle diffusion was not the controlling absorption mechanism [36]. The first stage occurs during the first 5 min. This is the fastest process and could be attributed to the instant adsorption in the pores of the material. As mentioned earlier, the MNPs could modify the hydrogel, increasing the porosity. This implies an increase in the specific area; in this first stage, the intraparticle diffusion had no relevance [40]. During the second stage, intraparticle diffusion took place, and finally, in the third stage, the adsorption rate decreased to reach the equilibrium because of the lower solute concentration [41].

Recovery and Reusability of Adsorbents

In the field of environmental remediation technologies, the challenge is to find materials with high adsorption capacity that may be easily removed from the contaminated media. From the economic point of view, it is desirable that such materials could be used for several cycles without losing their adsorption capability, or at least with minimal loss.

In the case of the ferrogels prepared in this work, their adsorption capability was tested along five consecutive adsorption–desorption cycles. The values obtained for PVA hydrogel and all ferrogels after five adsorption–desorption cycles are presented in Table 6, and correspond to the equilibrium situation.

These values were obtained recovering the gels in water, they seem to be lower than those previously reported [42], but in our case only distilled water was used, in several research work the recovery assays are done in special

Table 6 Absorption capacity (q_e) of the hydrogel and ferrogels after five adsorption–desorption cycles in water

After 5 cycles	Cu^{2+}					Cd^{2+}				
	PVA	1% MNPs	3% MNPs	6% MNPs	9% MNPs	PVA	1% MNPs	3% MNPs	6% MNPs	9% MNPs
Recovery %	91.6	69.7	83.9	87.3	84.5	78.8	90.8	88.5	84.0	87.7

solutions. It was considered that the addition of other salts generates a more complex effluent.

Conclusions

In this study, we propose the use of novel tools to eliminate heavy metals from water sources. Efficient adsorbents prepared by a simple, easy and low cost technique as freezing-thawing, with suitable properties in terms of their superparamagnetic behavior and large swelling capability. The potential of these materials as efficient adsorbents of heavy metal ions in water was verified. The concentration of MNPs on the PVA matrix was key to improve the adsorption capability. The adsorption kinetics was determined as pseudo-second order model, whereas the Langmuir model was the most appropriate to explain the behavior of the gels.

The ferrogels demonstrated high efficiency up to about five cycles, retaining about 80% of their initial adsorption capability. The recovered data allow us to infer that ferrogels with these properties could strongly contribute to the solution of waste water pollution.

Aknowledgements This study was supported by CONICET (National Scientific and Technical Research Council), ANPCyT (National Agency of Scientific and Technology Promotion), UNMdP (National University of Mar del Plata), UNS (University of South) and UNLP (University of La Plata).

References

1. Corcoran E (2010) Sick water?: the central role of wastewater management in sustainable development: a rapid response assessment. UNEP/Earthprint, Arendal
2. Woodard F (2001) Industrial waste treatment handbook. Butterworth-Heinemann, Oxford
3. Le NL, Nunes SP (2016) Sustain Mater Technol 7:1–28
4. Osińska M (2017) J Sol-Gel Sci Technol 81:678–692
5. Sabzi M, Samadi N, Abbasi F, Reza Mahdavinia G, Babaahmadi M (2017) Mater Sci Eng C 74:374–381
6. Hassan C, Peppas N (2000) Structure and applications of poly(vinyl alcohol) hydrogels produced by conventional crosslinking or by freezing/thawing methods, biopolymers PVA hydrogels, anionic polymerisation nanocomposites. Springer, Berlin Heidelberg
7. Gonzalez JS, Martinez YN, Castro GR, Alvarez VA (2016) Adv Mater Lett 7:640–645
8. Gonzalez JS, Ponce A, Alvarez VA (2016) Adv Mater Lett 7:979–985
9. Santos A, de Oliveira FWF, Silva FHA, Maria DA, Ardisson JD, de Almeida WA, Macêdo HEL, Palmieri MB, Franco (2012) Chem Eng J 210:432–443
10. Bruvera I, Hernández R, Mijangos C, Goya G (2015) J Magn Magn Mater 377:446–451
11. Muzzalupo R, Tavano L, Rossi CO, Picci N, Ranieri GA (2015) Colloids Surf B 134:273–278
12. Luo X, Zeng J, Liu S, Zhang L (2015) Bioresour Technol 194:403–406
13. Reza Mahdavinia G, Etemadi H (2014) Mater Sci Eng C 459:250–260
14. Reza Mahdavinia G, Mousanezhad S, Hosseinzadeh H, Darvishi F, Sabzi M (2016) Carbohydr Polym 147:379–391
15. Reza Mahdavinia G, Soleymani M, Etemadi H, Sabzi M, Atlas Z (2018) Int J Biol Macromol 107:719–729
16. Song W, Liu M, Hu R, Tan X, Li J (2014) Chem Eng J 246:268–276
17. Zrínyi M, Barsi L, Büki A (1997) Polym Gels Netw 5:415–427
18. Girginova PI, Daniel-da-Silva AL, Lopes CB, Figueira P, Otero M, Amaral VS, Pereira E, Trindade T (2010) J Colloid Interface Sci 345:234–240
19. Xu R, Zhou G, Tang Y, Chu L, Liu C, Zeng Z, Luo S (2015) Chem Eng J 275:179–188
20. Zheng S, Shin JY, Song SY, Yu SJ, Suh H, Kim I (2014) J Appl Polym Sci 131:40610
21. Ferrari E, Ranucci E, Edlund U, Albertsson A-C (2015) J Appl Polym Sci 132:41695
22. Mahmoud GA, Abdel-Aal SE, Badway NA, Elbayaa AA, Ahmed DF (2017) Polym Bull 74:337–358
23. Peppas NA, Merrill EW (1976) J Appl Polym Sci 20:1457–1465
24. Mc Gann MJ, Higginbotham CL, Geever LM, Nugent MJ (2009) Int J Pharm 372:154–161
25. Moscoso-Londoño O, Gonzalez JS, Muraca D, Hoppe CE, Alvarez VA, López-Quintela A, Socolovsky LM, Pirota KR (2013) Eur Polym J 49:279–289
26. Ricciardi R, Auriemma F, De Rosa C, Lauprêtre F (2004) Macromolecules 37:1921–1927
27. Gonzalez JS, Ludueña LN, Ponce A, Alvarez VA (2014) Mater Sci Eng C 34:54–61
28. Morris GE, Fornasiero D, Ralston J (2002) Int J Miner Process 67:211–227
29. Zhou L, He B, Zhang F, Facile (2011) ACS Appl Mater Interfaces 4:192–199
30. Lemine O, Omri K, Zhang B, El Mir L, Sajieddine M, Alyamani A, Bououdina M (2012) Superlattices Microstruct 52:793–799
31. Gonzalez J, Hoppe C, Muraca D, Sánchez F, Alvarez V (2011) Colloid Polym Sci 289:1839–1846
32. Singha NR, Mahapatra M, Karmakar M, Dutta A, Mondal H, Chattopadhyay PK (2017) Polym Chem 8:6750–6777
33. Mohammad N, Atassi Y, Tally M (2017) Polym Bull 74:4453
34. Yan J, Huang Y, Miao Y-E, Tjiu WW, Liu T (2015) J Hazard Mater 283:730–739
35. Paulino AT, Belfiore LA, Kubota LT, Muniz EC, Almeida VC, Tambourgi EB (2011) Desalination 275:187–196
36. Jamnongkan T, Kantarot K, Niemtang K, Pansila PP, Wattanakornsiri A (2014) Trans Nonferrous Met Soc China 24:3386–3393

37. Zhang D-k, Wang D-g, Duan J-j, Ge S-r (2009) J Bionic Eng 6:22–28
38. Mahdavinia GR, Massoudi A, Baghban A, Shokri E (2014) J Environ Chem Eng 2:1578–1587
39. Singh T, Singhal R (2014) Desalination Water Treat 52:5611–5628
40. Chen JH, Lin H, Luo ZH, He YS, Li GP (2011) Desalination 277:265–273
41. Tang SC, Yin K, Lo IM (2011) J Contaminant Hydrol 125:39–46
42. Hui B, Zhang Y, Ye L (2014) Chem Eng J 235:207–214
43. Mørup S, Hansen M, Frandsen C (2011) Comprehensive nanoscience and technology. In: Andrews DL, Scholes GD, Wiederrecht GP (eds) Magnetic nanoparticles, vol 12011, Elsevier, Oxford, pp 433–487
44. Bruvera IJ, Mendoza Zélis P, Pilar Calatayud M, Goya GF, Sánchez FH (2015) J Appl Phys 118:184304
45. Bedanta S, Kleemann W (2009) J Phys D 42:013001
46. Knobel M, Nunes W, Socolovsky L, De Biasi E, Vargas J, Denardin J (2008) J Nanosci Nanotechnol 8:2836–2857
47. Sánchez FH, Zélis PM, Arciniegas ML, Pasquevich GA, van Raap MF (2017) Phys Rev B 95:134421